IJSES
International Journal of Scientific Engineering and Science
Volume 10, Issue 8, pp. 15-21, August 2026. ISSN (Online): 2456-7361

Numerical Simulation of Steady Incompressible Flow Through a Stenosed Channel Using a Weak Galerkin Finite Element Method

Biao Yang[1], Jun Zhang[2], Peng Song[3]
[1]School of Mathematical Sciences, Guizhou Normal University, Guiyang, Guizhou, China-550025
[2]School of Mathematical Sciences, Guizhou Normal University, Guiyang, Guizhou, China-550025
[3]School of Mathematical Sciences, Guizhou Normal University, Guiyang, Guizhou, China-550025
Corresponding author: 804413215@qq.com

Abstract—*We evaluate a stabilized weak Galerkin (WG) discretization for steady incompressible flow in a smooth two-dimensional stenosed channel. The method uses element-interior P1 velocity, edgewise P0 velocity, elementwise P0 pressure, standard WG stabilization, skew-symmetric convection, and a centered natural-outlet correction, with no upwind term. A manufactured solution recovers the expected rates, and a Poiseuille test verifies the outlet treatment and mass conservation. A four-level mesh study adopts the finest available $N_y = 24$ grid. For $\delta = 0.4$, sampled Re = 20–200 cases show decreasing maximum speed and pressure difference; recirculation is detected only at Re = 150 and 200, so the sampled onset lies in $100 < Re \le 150$. At Re = 100, increasing δ from 0.2 to 0.5 raises speed, pressure difference, and wall shear; recirculation is detected only at $\delta = 0.5$, giving $0.4 < \delta \le 0.5$. The work is a numerical verification and sampled parameter study, not a critical-parameter or external-benchmark determination.*

Keywords—*Stenosed channel; incompressible flow; Navier–Stokes equations; skew-symmetric form; weak Galerkin method.*

I. Introduction

Smooth stenoses occur in ducts, microchannels, filters, and idealized arterial models. They accelerate the flow, alter pressure and wall shear, and may cause downstream separation; these effects depend on geometry and Reynolds number [7]–[9].

WG methods replace classical derivatives by discrete weak operators and use independent interior and boundary velocity unknowns, supporting discontinuous spaces and unstructured meshes [1]–[5]. Related developments include divergence-free, pressure-robust, and superconvergent WG schemes [10]–[12].

Zhang and Lin [4] analyzed a stabilized WG method for stationary Navier–Stokes equations, proving stability, conditional uniqueness, and optimal velocity-energy and pressure estimates. Their skew-symmetric convection form gives exact cancellation when its last two arguments coincide. This study extends that framework to a smooth open channel.

We assess the existing skew-symmetric, non-upwind WG implementation using a manufactured solution, a Poiseuille outlet test, and sampled channel cases with $Re \in \{20,50,100,150,200\}$ and $\delta \in \{0.2,0.3,0.4,0.5\}$. Reported quantities are speed, section-averaged pressure difference, wall shear, conservation, symmetry, and detected reverse flow.

Section II defines the problem, Section III the WG formulation, Section IV the solver and diagnostics, Section V verification and mesh sensitivity, Section VI results, and Section VII conclusions.

II. Governing Equations and Flow Configuration

A. Stationary incompressible Navier–Stokes equations

Let Ω be a bounded two-dimensional flow region with boundary $\partial\Omega$. The nondimensional stationary incompressible Navier–Stokes equations are

$$-\nu\Delta u + (u \cdot \nabla)u + \nabla p = f \quad in\ \Omega \qquad (1)$$

$$\nabla \cdot u = 0 \quad in\ \Omega \qquad (2)$$

Here $u = (u_1,u_2)^T$, p is pressure, f is body force, and $\nu > 0$ is kinematic viscosity. The natural outlet fixes the pressure reference in channel cases; the manufactured test uses zero-mean pressure. For the stenosed channel, f = 0 and $\nu = Re^{-1}$, based on unit unobstructed height and mean inlet speed.

B. Stenosed-channel geometry and boundary conditions

The channel has L = 12 and height $H\delta(x)$. A smooth stenosis centered at $x^c = 4$ with length $L_s = 2$ is defined by $H\delta(x) = 1 − (\delta/2)[1 + \cos(2\pi(x−x^c)/L_s)]$ for $|x−x^c| \le L_s/2$ and $H\delta(x) = 1$ otherwise. Thus the throat height is $1−\delta$; δ = 0.2, 0.3, 0.4, and 0.5.

A fully developed parabolic profile with unit mean velocity is prescribed at the inlet,

International Journal of Scientific Engineering and Science
Volume 10, Issue 8, pp. 15-21, August 2026. ISSN (Online): 2456-7361

$$u_1(0,y) = 6\left(\frac{1}{4} - y^2\right), \quad u_2(0,y) = 0, \quad -\frac{1}{2} < y < \frac{1}{2} \quad (3)$$

No slip is imposed on both walls and ν(∂u/∂n) − pn = 0 at x = 12. The seven-height downstream segment limits outlet influence near the stenosis. The δ = 0 channel provides the Poiseuille test.

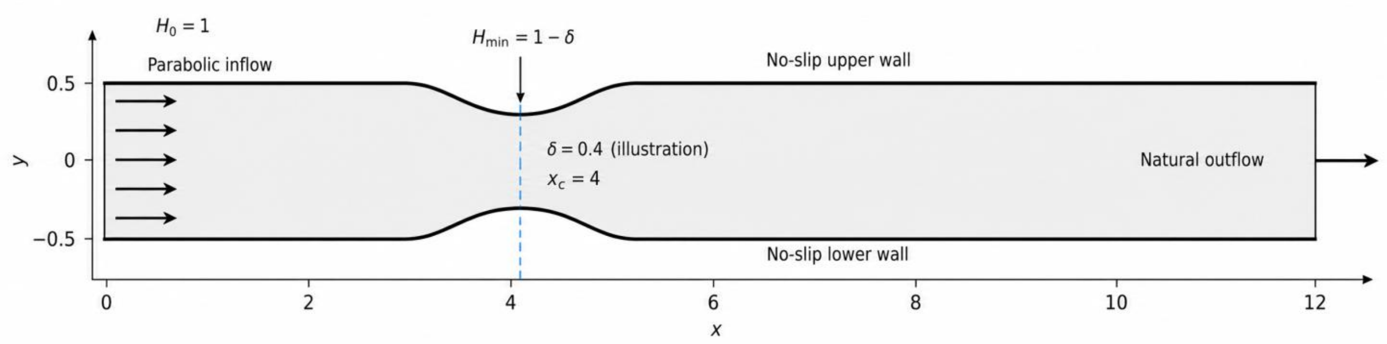

Fig. 1. Computational domain, smooth symmetric constriction, and boundary conditions for the stenosed-channel flow.

III. Weak Galerkin Finite Element Method

A. Discrete weak functions and differential operators

Let T_h be a shape-regular triangular or polygonal mesh. A weak function is $v = \{v_0, v_\beta\}$, with independent interior and edge components. For k ≥ 1, the local space is

$$W_{h,k}(T) = \{v = \{v_0, v_b\}: v_0 \in P_k(T), v_{b|_e} \in P_{k-1}(e)\} \quad (4)$$

The discrete weak gradient ∇wv ∈ [Pk−1(T)]² is defined by

$$(\nabla_w v, q)_T = -(v_0, \nabla \cdot q)_T + \langle v_b, q \cdot n \rangle_{\partial T} \quad (5)$$

For a vector weak function v = {v0,vb}, the discrete weak divergence divw v ∈ Pk−1(T) satisfies

$$(\nabla_w \cdot v, q)_T = -(v_0, \nabla q)_T + \langle v_b \cdot n, q \rangle_{\partial T} \quad (6)$$

B. Velocity–pressure spaces and stabilization

The edge component is single valued on each mesh edge. X_h^0 has zero edge values on Dirichlet boundaries, and X_h^g uses the projected inflow and wall data. The pressure spaces are

$M_h^0 = \{q \in L_0^2(\Omega): q|_T \in P_{k-1}(T), T \in T_h\}$, manufactured/full-Dirichlet case (7a)

$M_h^{out} = \{q \in L^2(\Omega): q|_T \in P_{k-1}(T), T \in T_h\}$, open-channel case (7b)

The diffusion form contains the discrete weak gradient and the standard weak Galerkin stabilization,
We use k = 1: $u_0|_t \in [P_1(T)]^2$, $u_\beta|_e \in [P_0(e)]^2$, and $p_h|_t \in P_0(T)$; weak gradients and divergences are elementwise constant.

$$a_h(u,v) = (\nabla_w u, \nabla_w v)_h + s_h(u,v) \quad (8)$$

$$s_h(u,v) = \sum_T h_T^{-1} \langle Q_b u_0 - u_b, Q_b v_0 - v_b \rangle_{\partial T} \quad (9)$$

Term (9) is the standard WG consistency stabilization, not an upwind or convection-dependent term.

C. Skew-symmetric convective form

For w,u,v ∈ Xh, the nonlinear contribution is discretized by the skew-symmetric trilinear form

$$b_h(w;u,v) = \frac{1}{2}\big((w_0 \cdot \nabla_w)u, v_0\big)_h - \frac{1}{2}\big((w_0 \cdot \nabla_w)v, u_0\big)_h (10)$$

The identity $b_h(w;v,v) = 0$ gives the closed-boundary energy cancellation [6].

D. Skew-consistent natural-outlet correction

At an open outlet, the implementation adds the centered correction

$$c_{out}(w;u,v) = \frac{1}{2}\langle (w_b \cdot n)u_b, v_b \rangle_{\Gamma_{out}} = \frac{1}{2}\sum_{e \subset \Gamma_{out}} \sum_q w_q \big(w_b(x_q) \cdot n_e\big)\big(u_b(x_q) \cdot v_b(x_q)\big) \quad (10a)$$

$$c_h(w;u,v) = b_h(w;u,v) + c_{out}(w;u,v) \quad (10b)$$

Here n_e is the outward outlet normal; u_β, v_β, and w_β are edge traces, and wq includes edge length. The coefficient and sign match the code. The term is centered and contains no upwinding, artificial viscosity, edge penalty, or one-sided flux.

IJSES

International Journal of Scientific Engineering and Science

Volume 10, Issue 8, pp. 15-21, August 2026. ISSN (Online): 2456-7361

E. Discrete formulation

The open-channel solution $(u_h,p_h) \in X_h^g \times M_h^{out}$ satisfies

$$a_h(u_h, v) + c_h(u_h; u_h, v) - (p_h, div_w v) = (f, v_0) \quad (11)$$

$$(div_w u_h, q_h) = 0 \quad (12)$$

For homogeneous Dirichlet data, the velocity–pressure pair in [4] satisfies a mesh-independent discrete inf–sup condition. Under the regularity and small-data hypotheses stated there, the discrete problem has a stable solution and the solution is unique when $C0N0\|f\|/\nu^2 < 1$. If $u \in [Hk+1(\Omega)]^2$ and $p \in Hk(\Omega)$, the theoretical estimate has the form

$$\|\nabla u - \nabla_w u_h\|_h + \|p - p_h\|_0 \le Ch^k(\|u\|_{k+1}^2 + \|p\|_k) \quad (13)$$

Inflow and no-slip data are imposed through edge unknowns, while outlet edges remain free. The natural outlet provides the pressure reference without a mean-pressure multiplier; the manufactured test uses M_h^0. A mixed-boundary theory is not developed here.

IV. Nonlinear Solver and Implementation

A. Newton linearization

At iterate (u_h^m,p_h^m), Newton uses $c_h(u_h^m;\delta u_h^m,v) + c_h(\delta u_h^m;u_h^m,v)$, including both outlet-trace derivatives. The update is $X^{m+1} = X^m + \lambda_m \delta X^m$, with backtracking only when the residual decrease test fails.

The monitored quantities are $r\_abs^m = \|R(X^m)\|_2$, $r\_rel^m = \|R(X^m)\|_2/\max(\|R(X^0)\|_2,eps)$, and $s\_upd^m = \|\lambda_m \delta X^m\|_2/\max(\|X^m\|_2,1)$. The stopping test is (14); final relative residuals are below 3×10^{-13}.

$$(r\_abs^m \le 10^{-10} \text{ or } r\_rel^m \le 10^{-8})$$
$$s\_upd^m \le 10^{-10}. \quad (14)$$

For channel cases, the natural outlet fixes the pressure reference and no zero-mean constraint is imposed. The manufactured test uses zero-mean pressure. Dirichlet edge velocities are eliminated strongly, and the existing quadrature rules are retained.

B. Reynolds-number continuation

Stokes flow initializes continuation. Each converged solution seeds the next Reynolds number or stenosis ratio; only the initial guess changes.

C. Postprocessing quantities

The reported speed is $|u|_{max} = \max_\Omega \mathrm{hypot}(u_1,u_2)$, evaluated from the interior P1 field with eighth-order triangular quadrature. The global maximum is replaced by the $x \le L-1$ maximum only when an outlet-layer value exceeds it by more than 2%. Section-averaged pressure gives $\Delta p = \bar{p}(2)-\bar{p}(8)$, which includes both background viscous and constriction effects. Signed wall shear is $\tau w = \nu t\cdot(\nabla u+\nabla u^T)n$, and mass imbalance is $|Qin-Qout|/|Qin|$.

Recirculation is searched on 1191 streamwise and 101 wall-normal samples. A downstream wall interval is accepted only when at least three consecutive points fall below $-\max(10^{-8},10^{-5}\max|u_1|)$, its length exceeds $\max(2\Delta x,0.5\min_t h_t)$, and the wall-referenced streamfunction excursion exceeds $\max(10^{-10},10^{-5}\max|\psi upper-\psi lower|)$. Separation and reattachment are linearly interpolated, with $L_r = x_r-x_s$ evaluated on each wall. Thus reported onset values are sampled detections, not critical thresholds.

V. Numerical Verification

A. Manufactured solution

On $\Omega = (0,1)^2$, the divergence-free manufactured solution is

$$u_1(x,y) = x^2(1-x)^2(2y-6y^2+4y^3),$$
$$u_2(x,y) = -(2x-6x^2+4x^3)y^2(1-y)^2. \quad (15)$$
$$p(x,y) = x^3 - y^3. \quad (16)$$

The velocity generated by $\psi = x^2(1-x)^2y^2(1-y)^2$ is divergence free and vanishes on $\partial\Omega$; $p = x^3-y^3$ has zero mean. With $f = -\nu\Delta u + (u\cdot\nabla)u + \nabla p$, Table I gives approximately second-order interior-velocity L^2 convergence and first-order energy and pressure L^2 convergence.

TABLE I. ERRORS AND CONVERGENCE RATES FOR THE MANUFACTURED SOLUTION.

h	$\|Q_0u-u_0\|_0$	rate	$\|\|\|Qhu-uh\|\|\|$	rate	$\|Qp-ph\|_0$	rate
1/10	5.187920×10^{-2}	—	4.148413×10^{-1}	—	3.853013×10^{-2}	—
1/20	1.313725×10^{-2}	1.98	2.133209×10^{-1}	0.96	1.911708×10^{-2}	1.01
1/40	3.298409×10^{-3}	1.99	1.076315×10^{-1}	0.99	9.524825×10^{-3}	1.01
1/80	8.257108×10^{-4}	2.00	5.396893×10^{-2}	1.00	4.755182×10^{-3}	1.00

Volume 10, Issue 8, pp. 15-21, August 2026. ISSN (Online): 2456-7361

B. *Mesh-sensitivity study*

A four-level mesh-sensitivity study at Re = 100 and $\delta = 0.4$ uses $N_\gamma = 12$, 16, 20, and 24. The reported h is the maximum element diameter in $3 \le x \le 5$. All cases converge with near-machine-precision absolute residuals, final relative residuals below 3×10^{-13}, and machine-precision flow-rate balance.

TABLE II. MESH-SENSITIVITY RESULTS AT Re = 100 AND $\delta = 0.4$.

Mesh	N_γ	h near throat	Elements	Velocity DOFs	Pressure DOFs	$\lvert u\rvert_{max}$	Δp	Mass error
Coarse	12	0.110304	3456	31416	3456	2.344514	1.458711	0
Medium-1	16	0.082961	6208	56292	6208	2.250624	1.407365	2.22×10^{-16}
Medium-2	20	0.066479	9680	87644	9680	2.231702	1.365793	2.22×10^{-16}
Fine	24	0.055483	13824	125040	13824	2.220541	1.340062	4.44×10^{-16}

From $N_\gamma = 20$ to 24, $\lvert u\rvert_{max}$ and maximum wall shear change by 0.503% and 0.983%, while Δp changes by 1.920%. Strict mesh independence is therefore not claimed. The finest available $N_\gamma = 24$, $N_x = 288$ mesh (13,824 elements) is used for all sampled parameter cases.

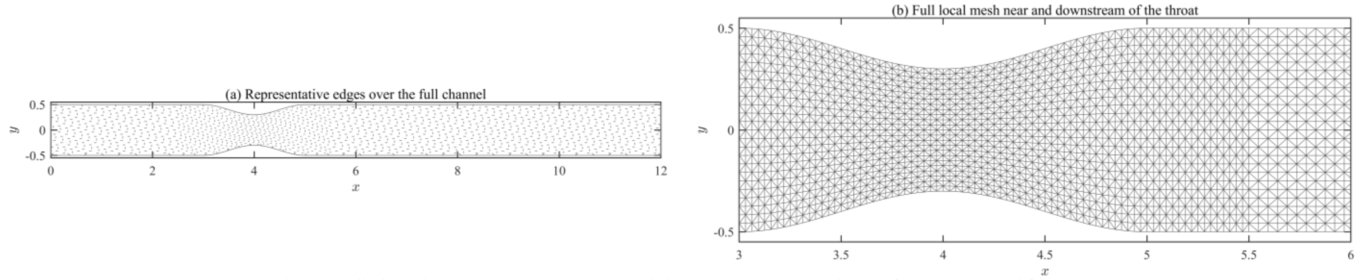

Fig. 2. Full-domain representative edges and throat-region triangulation for $N_\gamma = 24$ and $\delta = 0.4$.

VI. Stenosed-Channel Results

A. *Straight-channel Poiseuille verification*

The $\delta = 0$ channel verifies the inflow, centered outlet correction, pressure reconstruction, mass conservation, and removal of the outlet speed artifact. For unit mean inflow, $u_1 = 6(1/4-y^2)$, $u_2 = 0$, and $dp/dx = -0.12$.

On $N_\gamma = 16$, the final residual is 1.81×10^{-15} and the flow-rate imbalance is 2.22×10^{-16}. The computed maximum speed is 1.55833 versus 1.5, a 3.89% error. Velocity L^2, energy, and pressure L^2 errors are 0.10703, 3.19955, and 0.19440. The section pressure difference is 0.770219 versus 0.72, and the fitted slope is -0.12857.

From $N_\gamma = 12$ to 16, the observed velocity L^2, energy, and pressure L^2 rates are 1.125, 0.392, and 0.568; this short sequence is not used to claim asymptotic optimality.

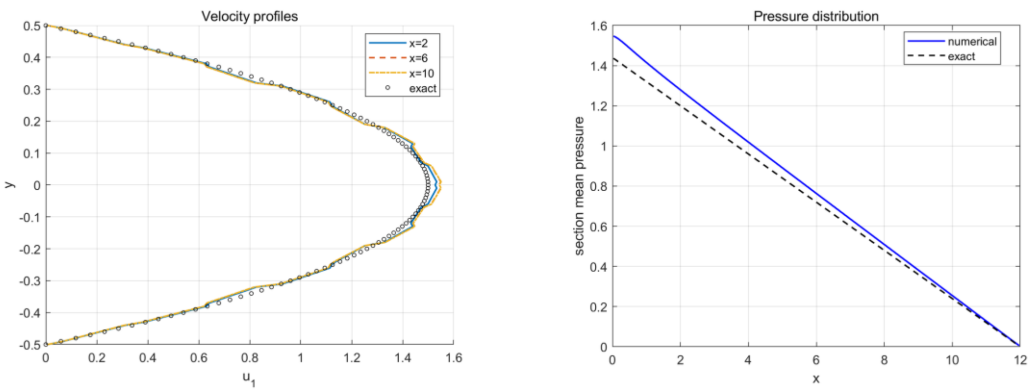

Fig. 3. Poiseuille verification on $N_\gamma = 16$: velocity profiles and section-averaged pressure.

B. *Effect of Reynolds number*

The Reynolds study uses $\delta = 0.4$ and the $N_\gamma = 24$, $N_x = 288$ mesh at Re = 20, 50, 100, 150, and 200. Mean inflow remains one and $\nu = 1/\mathrm{Re}$. Final relative residuals are below 3×10^{-13}, divergence errors are $O(10^{-14})$, and mass errors are at most 4.44×10^{-16}.

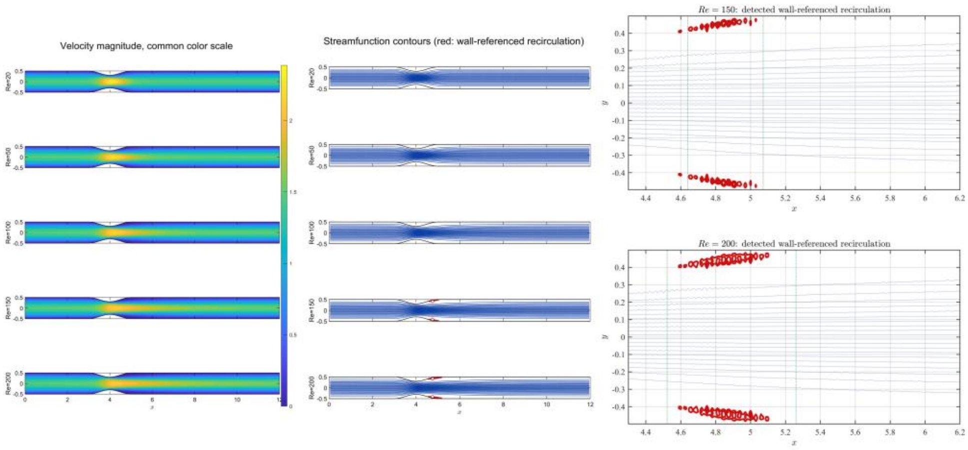

Fig. 4. Velocity magnitude, streamfunction contours, and downstream recirculation zooms for the sampled Reynolds numbers at δ = 0.4.

TABLE III. EFFECT OF THE REYNOLDS NUMBER AT δ = 0.4.

Re	$\lvert u\rvert_{max}$	$x(\lvert u\rvert_{max})$	Δp	max|τw|	Recirc.	L_r	Mass error
20	2.398369	4.094370	5.455812	1.028254	No	—	2.22×10^{-16}
50	2.305614	4.218142	2.324627	0.485419	No	—	4.44×10^{-16}
100	2.220541	4.218142	1.340062	0.290782	No	—	4.44×10^{-16}
150	2.179453	4.280642	1.055159	0.217154	Yes	0.432035	2.22×10^{-16}
200	2.154561	4.280642	0.936064	0.176815	Yes	0.738588	4.44×10^{-16}

As Re increases, ν decreases. Across the samples, $\lvert u\rvert_{max}$ falls from 2.398369 to 2.154561, Δp from 5.455812 to 0.936064, and max|τw| from 1.028254 to 0.176815. Recirculation is detected only at Re = 150 and 200, with L_r = 0.432035 and 0.738588. Hence the sampled onset is bracketed by 100 < Re ≤ 150.

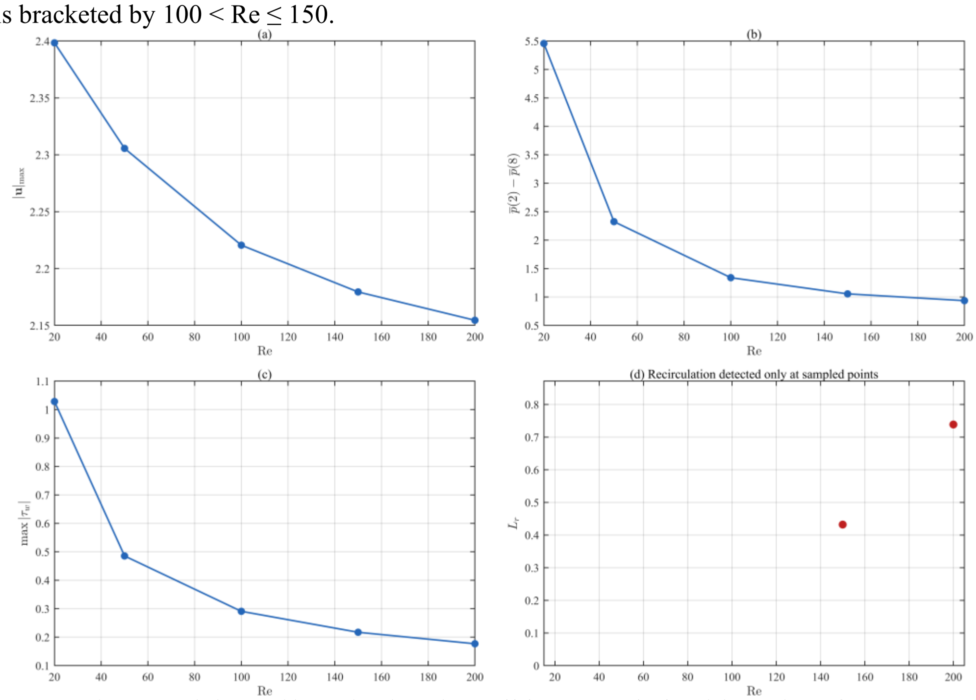

Fig. 5. Sampled Reynolds-number dependence of $\lvert u\rvert_{max}$, Δp, max|τw|, and detected L_r at δ = 0.4.

Volume 10, Issue 8, pp. 15-21, August 2026. ISSN (Online): 2456-7361

C. Effect of stenosis ratio

At Re = 100, δ = 0.2, 0.3, 0.4, and 0.5 are computed on the N_γ = 24 mesh. In all cases Qin = Qthroat = Qout = 1, and mean throat speeds agree with $1/(1-\delta)$ to about 3.4×10^{-14}.

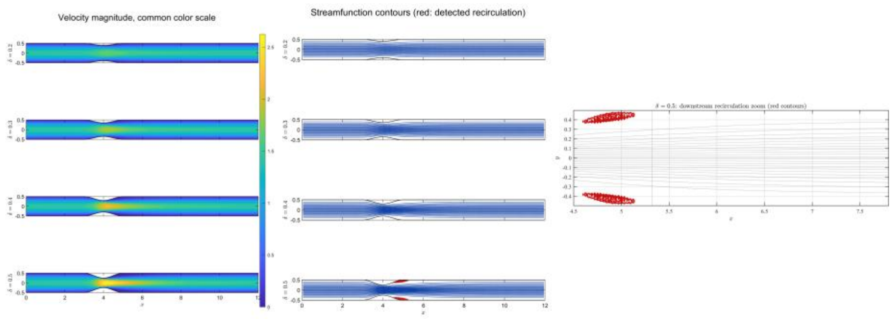

Fig. 6. Velocity magnitude, streamfunction contours, and the δ = 0.5 downstream zoom at Re = 100.

TABLE IV. EFFECT OF THE STENOSIS RATIO AT Re = 100.

δ	H_{min}	$\|u\|_{max}$	$x(\|u\|_{max})$	Δp	$\max\|\tau w\|$	Recirc.	L_r	Mass error
0.2	0.8	1.758866	4.280642	0.898947	0.134389	No	—	2.22×10^{-16}
0.3	0.7	1.947073	4.280642	1.054602	0.196297	No	—	4.44×10^{-16}
0.4	0.6	2.220541	4.218142	1.340062	0.290782	No	—	4.44×10^{-16}
0.5	0.5	2.629923	4.219370	1.901624	0.443899	Yes	0.861143	0

Across the sampled δ values, $|u|_{max}$ rises from 1.758866 to 2.629923, Δp from 0.898947 to 1.901624, and $\max|\tau w|$ from 0.134389 to 0.443899. The pressure difference includes background viscous and constriction effects. Recirculation is detected only at δ = 0.5, where L_r = 0.861143; the sampled onset is therefore bracketed by $0.4 < \delta \le 0.5$.

Pressure and wall-shear symmetry errors are $O(10^{-16})$ and $O(10^{-15})$, while velocity symmetry errors are 1.16×10^{-4}–1.67×10^{-4}.

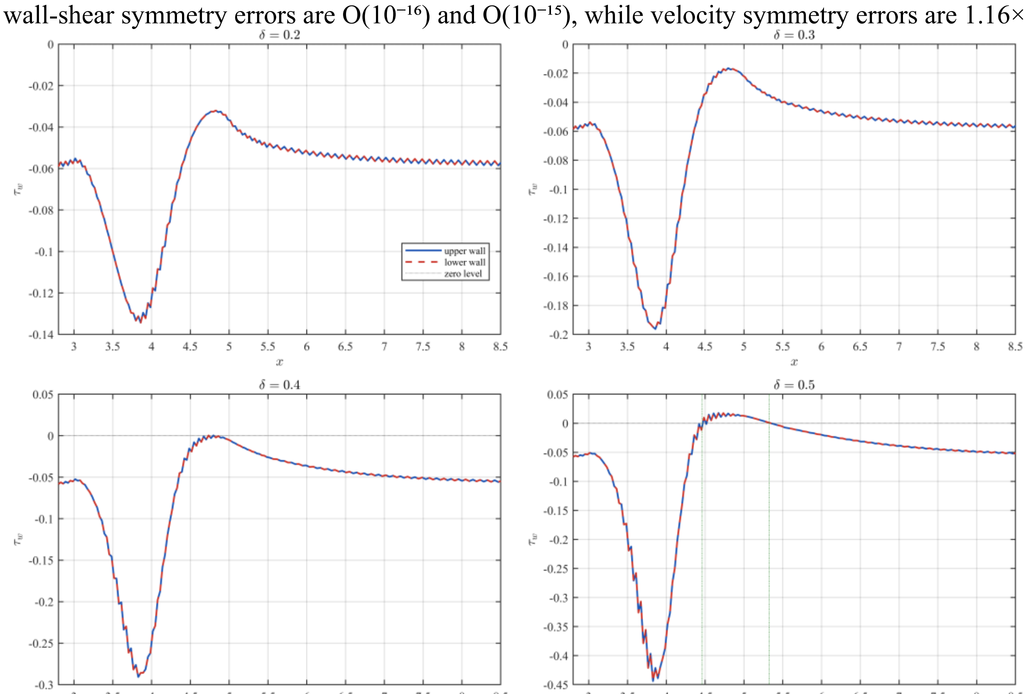

Fig. 7. Signed wall shear for the sampled stenosis ratios at Re = 100; δ = 0.5 separation and reattachment are marked.

International Journal of Scientific Engineering and Science
Volume 10, Issue 8, pp. 15-21, August 2026. ISSN (Online): 2456-7361

D. Reference-case diagnostics

Table V lists numerical diagnostics for Re = 100, δ = 0.4, and $N_\gamma = 24$; physical quantities are already in Tables III and IV.

TABLE V. NUMERICAL DIAGNOSTICS AT Re = 100 AND δ = 0.4.

Diagnostic quantity	WG result	Purpose
Relative flow-rate imbalance	4.44×10^{-16}	Mass conservation
Discrete divergence error	2.71×10^{-14}	Incompressibility
Final absolute Newton residual	2.413×10^{-15}	Nonlinear convergence
Final relative Newton residual	9.967×10^{-14}	Scaled convergence
Maximum wall velocity	0	No-slip enforcement
Velocity symmetry error	1.44×10^{-4}	Field symmetry
Pressure symmetry error	4.07×10^{-16}	Pressure symmetry
Wall-shear symmetry error	1.96×10^{-15}	Wall diagnostic symmetry

E. Discussion

The manufactured and Poiseuille tests verify convergence, boundary treatment, pressure reconstruction, and conservation. The mesh study shows that Δp is more refinement-sensitive than speed or wall shear; $N_\gamma = 24$ is the finest available common mesh, not a mesh-independent limit.

With unit mean inflow, increasing Re lowers ν, Δp, and wall-shear magnitude, while recirculation is detected only at sampled Re ≥ 150. At Re = 100, speed, Δp, and wall shear increase with δ, and recirculation is detected only at δ = 0.5. These sampled brackets are not critical-parameter estimates.

VII. Conclusion

A skew-symmetric WG method with a centered natural-outlet correction has been tested for steady flow through a smooth stenosed channel. Manufactured and Poiseuille cases verify convergence, outlet treatment, and conservation; the finest available common mesh is $N_\gamma = 24$, $N_x = 288$.

All sampled cases converge with final relative residuals below 3×10^{-13} and mass errors below 5×10^{-16}. Recirculation is detected at Re = 150 and 200 for δ = 0.4, and only at δ = 0.5 for Re = 100, giving sampled onset brackets 100 < Re ≤ 150 and 0.4 < δ ≤ 0.5. The reported Δp includes background viscous and constriction effects. These results are a numerical verification and sampled parameter study, not a critical-parameter or external-benchmark validation.

References

[1] J. Wang and X. Ye, “A weak Galerkin finite element method for second-order elliptic problems,” Journal of Computational and Applied Mathematics, vol. 241, pp. 103–115, 2013.
[2] J. Wang and X. Ye, “A weak Galerkin finite element method for the Stokes equations,” Advances in Computational Mathematics, vol. 42, pp. 155–174, 2016.
[3] X. Liu, J. Li, and Z. Chen, “A weak Galerkin finite element method for the Navier–Stokes equations,” Journal of Computational and Applied Mathematics, vol. 333, pp. 442–457, 2018.
[4] T. Zhang and T. Lin, “An analysis of a weak Galerkin finite element method for stationary Navier–Stokes problems,” Journal of Computational and Applied Mathematics, vol. 362, pp. 484–497, 2019.
[5] X. Hu, L. Mu, and X. Ye, “A weak Galerkin finite element method for the Navier–Stokes equations,” Journal of Computational and Applied Mathematics, vol. 362, pp. 614–625, 2019.
[6] V. Girault and P.-A. Raviart, Finite Element Methods for Navier–Stokes Equations: Theory and Algorithms. Berlin, Germany: Springer-Verlag, 1986.
[7] D. F. Young and F. Y. Tsai, “Flow characteristics in models of arterial stenoses—I. Steady flow,” Journal of Biomechanics, vol. 6, no. 4, pp. 395–410, 1973.
[8] B. D. Seeley and D. F. Young, “Effect of geometry on pressure losses across models of arterial stenoses,” Journal of Biomechanics, vol. 9, no. 7, pp. 439–448, 1976.
[9] S. A. Ahmed and D. P. Giddens, “Velocity measurements in steady flow through axisymmetric stenoses at moderate Reynolds numbers,” Journal of Biomechanics, vol. 16, no. 7, pp. 505–516, 1983.
[10] L. Mu, J. Wang, X. Ye, and S. Zhang, “A discrete divergence-free weak Galerkin finite element method for the Stokes equations,” Applied Numerical Mathematics, vol. 125, pp. 172–182, 2018.
[11] L. Mu, “A pressure-robust weak Galerkin finite element method for Navier–Stokes equations,” Numerical Methods for Partial Differential Equations, vol. 39, pp. 2327–2354, 2023.
[12] P. Xie and P. Zhu, “Superconvergence of a weak Galerkin method for the Stokes equations with continuous pressure,” Applied Numerical Mathematics, vol. 179, pp. 27–38, 2022.